N63 20535

CONFIDENTIAL

Copy 659

NASA TM X-373

OTS PRICE
XEROX $ 4.60
MICROFILM $ 1.46

TECHNICAL MEMORANDUM

X-373

FREE-FLIGHT MEASURMENTS OF STATIC AND DYNAMIC STABILITY OF MODELS OF THE PROJECT MERCURY RE-ENTRY CAPSULE AT MACH NUMBERS 3 AND 9.5

By Simon C. Sommer, Barbara J. Short, and
Dale L. Compton

Ames Research Center
Moffett Field, Calif.

CLASSIFICATION CHANGED FROM
CONFIDENTIAL TO UNCLASSIFIED--
AUTHORITY NASA-CON 5-EFFECTIVE
17 JULY 63, JIM CARROLL
DOC. INC.

CLASSIFIED DOCUMENT - TITLE UNCLASSIFIED

This material contains information affecting the national defense of the United States within the meaning of the espionage laws, Title 18, U.S.C., Secs. 793 and 794, the transmission or revelation of which in any manner to an unauthorized person is prohibited by law.

NATIONAL AERONAUTICS AND SPACE ADMINISTRATION
WASHINGTON

August 1960

CONFIDENTIAL

0378128J030

DECLASSIFIED

NATIONAL AERONAUTICS AND SPACE ADMINISTRATION

TECHNICAL MEMORANDUM X-373

FREE-FLIGHT MEASUREMENTS OF STATIC AND DYNAMIC STABILITY OF MODELS OF THE PROJECT MERCURY RE-ENTRY CAPSULE AT MACH NUMBERS 3 AND 9.5*

By Simon C. Sommer, Barbara J. Short, and
Dale L. Compton

SUMMARY

Experimental measurements of the dynamic stability of scaled models of the Mercury re-entry capsule in free flight at constant altitude were made at Mach numbers near 3 and 9.5. It was found that the capsule is dynamically unstable at these Mach numbers, and that the flow conditions over the afterbody have a strong effect on the dynamic-stability characteristics.

Static stability and drag were measured at Mach numbers from 3 to 14. It was found that the capsule is statically stable throughout the angle-of-attack range tested and the total-drag coefficient is invariant with Mach number.

INTRODUCTION

After orbiting the earth, the Project Mercury capsule will re-enter the earth's atmosphere on a shallow-angle trajectory with zero lift. Studies of the oscillatory behavior of nonlifting vehicles entering the earth's atmosphere have indicated that divergent oscillations can begin near the altitude at which dynamic pressure is a maximum (ref. 1). Whether divergent oscillations will or will not begin at this altitude depends on the aerodynamic damping of the vehicle.

In support of Project Mercury, an investigation was conducted to determine the static- and dynamic-stability characteristics of the re-entry vehicle at two supersonic Mach numbers, approximately 3 and 9.5. The Reynolds numbers were nominally full-scale values. In addition to

*Title, Unclassified

the stability of the capsule, the drag was also investigated. The investigation was conducted in the Ames Supersonic Free-Flight Wind Tunnel and Ames Pressurized Ballistic Range. The results of this investigation are presented herein.

SYMBOLS

A	frontal area, sq ft
C_D	drag coefficiant, $\frac{\text{drag}}{q_\infty A}$, dimensionless
C_{L_α}	lift-curve slope, per radian
C_m	pitching-moment coefficient, $\frac{\text{pitching moment}}{q_\infty Ad}$, dimensionless
C_{m_α}	pitching-moment-curve slope, per radian
$C_{m_q} + C_{m_{\dot{\alpha}}}$	damping-in-pitch derivative, $\frac{\partial C_m}{\partial q(d/V)} + \frac{\partial C_m}{\partial \dot{\alpha}(d/V)}$, dimensionless
d	maximum body diameter, ft
I_y	transverse moment of inertia, $m\sigma^2$, slug-ft^2
$K_{1,2,3}$	constants in equation (1), deg
m	mass of model, slugs
M	Mach number, dimensionless
p	roll parameter, $\frac{\text{roll rate}}{\text{velocity}}$, radians/ft
q	angular pitching velocity, radians/sec
q_∞	free-stream dynamic pressure, lb/sq ft
R	Reynolds number based on maximum diameter, dimensionless
V	velocity along flight path, ft/sec
x	distance along flight path, ft
x_{cg}	axial distance from model nose to center-of-gravity position, ft

A 3 7 1

DECLASSIFIED

α	angle of pitch (in the vertical plane), deg
α_{m_i}	initial value of maximum-angle envelope, deg (see sketch (a))
α_{min_i}	initial value of minimum-angle envelope, deg (see sketch (a))
α_{m_f}	value of maximum-angle envelope at end of flight, deg (see sketch (a))
β	angle of yaw (in the horizontal plane), deg
$\eta_{1,2}$	damping exponents in equation (1), ft^{-1}
λ	wave length of pitching oscillation, ft/cycle
ρ	free-stream air density, slugs/cu ft
σ	transverse radius of gyration, ft
$\omega_{1,2}$	rates of rotation of vectors which describe the model pitching motion, radians/ft
$\frac{\omega d}{V}$	reduced frequency, dimensionless
ξ	dynamic-stability parameter, $C_D - C_{L_\alpha} + (C_{m_q} + C_{m_{\dot{\alpha}}})(d/\sigma)^2$, dimensionless

Superscript

$(\dot{})$	first derivative with respect to time

EXPERIMENTS

All of the data presented in this report were obtained by firing scaled models through enclosed free-flight facilities and recording the model motions. The basic data required for stability and drag evaluation are angle-of-attack and time-distance histories which are recorded by spark shadowgraphs and chronographs. The static and dynamic stability were obtained from the angle-of-attack histories which were analyzed to define the wave length of oscillation and the growth or decay of the pitching motion. Total-drag coefficients were computed from deceleration data obtained from the time-distance histories. Two facilities were utilized for the tests, the Ames Pressurized Ballistic Range and the Ames Supersonic Free-Flight Wind Tunnel. The ballistic range is equipped with 24 spark-shadowgraph stations located at various intervals along its

03791284 0390

203-foot length. Chronographs record the time intervals between shadowgraphs taken as the model passes each station. The wind tunnel is similar to the range except that the models are fired through a counter-current air stream. The test section of this wind tunnel is equipped with 9 spark-shadowgraph stations spaced at 3-foot intervals. The wind tunnel is described in more detail in reference 2.

Models and Test Conditions

A sketch of the model is shown in figure 1. The center of gravity of the models was located at either 35 percent or 51 percent of the diameter from the nose. The forward center-of-gravity position corresponded to the center-of-gravity location of the full-scale vehicle design at the time the tests were started. The noses of the models were machined from phosphor bronze, while the afterbodies were machined from 7075-T6 aluminum. With the strong possibility that the center-of-gravity location in the full-scale vehicle would be shifted aft, it was desirable that a model with a more rearward center-of-gravity location also be tested. The models for these tests were machined from titanium, with the center of gravity located at the center of volume. The front faces of all models except one were polished to a maximum surface roughness of about 20 microinches. The spike shown on the back of the model (fig. 1) was an aid used in measuring the angular orientation of the model from the shadowgraphs. The screw threads were used to hold the model in the sabot during launching. Figure 2 is a photograph of two models in their sabots. The nylon sabots were made in two pieces so that they would separate from the model at the gun muzzle. The model axes were inclined to the sabot axes with angles from 0° to 4°, which induced angles of attack to the model from 2° to 24°. The larger model shown in figure 2 had a 1.65-inch diameter, and the smaller model had a 0.45-inch diameter.

A 3 7 1

The larger models were used for the Mach number 3 tests which were conducted in the ballistic range. These models were launched from a 1.75-inch-diameter smooth-bore gun through still air. The static pressure in the ballistic range was 11.8 psia which resulted in a nominal Reynolds number of 2.2×10^6 based on free-stream conditions and model diameter. The average velocity of the models in the test section was 3200 feet per second. A typical variation of Reynolds number and Mach number with distance along the flight path is shown in figure 3(a).

The smaller models were used for the higher Mach number tests in which the models were launched upstream through a Mach number 3 air stream in the wind tunnel. Mach number 9.5 was obtained by launching the models with an average velocity of 4200 feet per second from a 0.50 caliber smooth-bore gun. The nominal Reynolds number of these tests was 1.4×10^6. A typical variation of Mach number and Reynolds number with distance along the flight path for these tests is shown in figure 3(b).

DECLASSIFIED

A limited number of tests were conducted at a Mach number of 14. This Mach number was obtained by launching the models with an average velocity of 7500 feet per second from a 37-mm shock-heated helium gun (ref. 3). The nominal Reynolds number for these tests was 1.9×10^6.

Stability Data Reduction

Stability data were obtained from analyses of the pitching and yawing motions of the models. The growth or decay of the motion is a measure of the dynamic stability, whereas the wave length of oscillation is a measure of the static stability. Stability parameters were obtained by fitting the following equation to the measurements of α and β of each flight,

$$\beta + i\alpha = K_1 e^{(\eta_1 + i\omega_1)x} + K_2 e^{(\eta_2 - i\omega_2)x} + K_3 e^{ipx} \qquad (1)$$

Equation (1) is the solution of the linear differential equation of motion as given in reference 4 and rewritten here in the nomenclature of this report. This equation includes the effects of model spin and trim angle on the motion.

The dynamic stability was determined from the constants η_1 and η_2 by means of the relation

$$\eta_1 + \eta_2 = \frac{\rho A}{2m} \xi \qquad (2)$$

where

$$\xi = C_D - C_{L_\alpha} + (C_{m_q} + C_{m_{\dot{\alpha}}})(d/\sigma)^2 \qquad (3)$$

It has been shown in references 5, 6, and 7 that ξ, in the form shown in equation (3), is a convenient parameter which describes the dynamic stability of a vehicle in free flight at constant altitude. The values of ξ presented in this report were calculated with the assumption of a linear system over the angle-of-attack range covered by any one flight. Each value of ξ, therefore, is the dynamic-stability parameter of an equivalent linear system whose amplitude of oscillation would grow or diminish in the same way as that experienced by the model.

03191284 1094

The static-stability derivative was computed from the wave length of oscillation by means of the following relation (ref. 6),

$$C_{m_\alpha} = -\frac{8\pi^2 I_y}{\lambda^2 \rho A d} \tag{4}$$

where

$$\lambda = \frac{2\pi}{\sqrt{\omega_1 \omega_2}} \tag{5}$$

Illustrations of the types of motions encountered in the present tests, as viewed in the α - β plane, are shown in figure 4. It can be seen that, in general, the data show precessing elliptical motions and that the angle range through which the model oscillates differs for each flight. The curves shown in the figure were obtained by use of equation (1). The curves in figures 4(a) and (b) were obtained by dividing each trajectory into two parts, each approximately 100 feet long and consisting of about 2-1/2 cycles of oscillation. Equation (1) was then fitted to the data from each half of each flight.[1] Every flight in the Mach number 3 tests was divided in this manner; thus, two values of ξ and C_{m_α} were obtained for each model flight in the ballistic range. This was done to reduce the effects of Mach number and Reynolds number variations and the effects of possible nonlinearities in the aerodynamic moments on the parameters which were calculated with the assumption of constant aerodynamic coefficients. It was not possible to divide the trajectories from the wind-tunnel tests (figs. 4(c) and (d)) since these flights consisted of less than two cycles of oscillation.

A 3 7 1

[1]For example, the first half of the motion shown in figure 4(a) was obtained from data from stations 1 through 13, and the second half of the motion from data from stations 12 through 24.

DECLASSIFIED

RESULTS AND DISCUSSION

Experimental measurements of stability and drag of the Mercury re-entry capsule are summarized in table I. The Mach numbers and Reynolds numbers listed in the table are average values for the flight or part of flight for which they are recorded. As was mentioned previously, the ballistic-range flights were divided into two parts; thus, for example, the first part of flight test number 52 is recorded in table I(a) as test number 52-1 and the last part as 52-2. The measured aerodynamic parameters are recorded as ξ, C_{m_α}, and C_D. The angles through which the models oscillated in each flight are indicated in the table where the initial value of the maximum-angle envelope, α_{m_i}, the final value of the maximum-angle envelope at the end of the flight, α_{m_f}, and the initial minimum-angle envelope, α_{min_i}, are recorded. These angles are illustrated in sketch (a) below. The reduced frequency, $\omega d/V$, and pertinent model measurements are also recorded in the table.

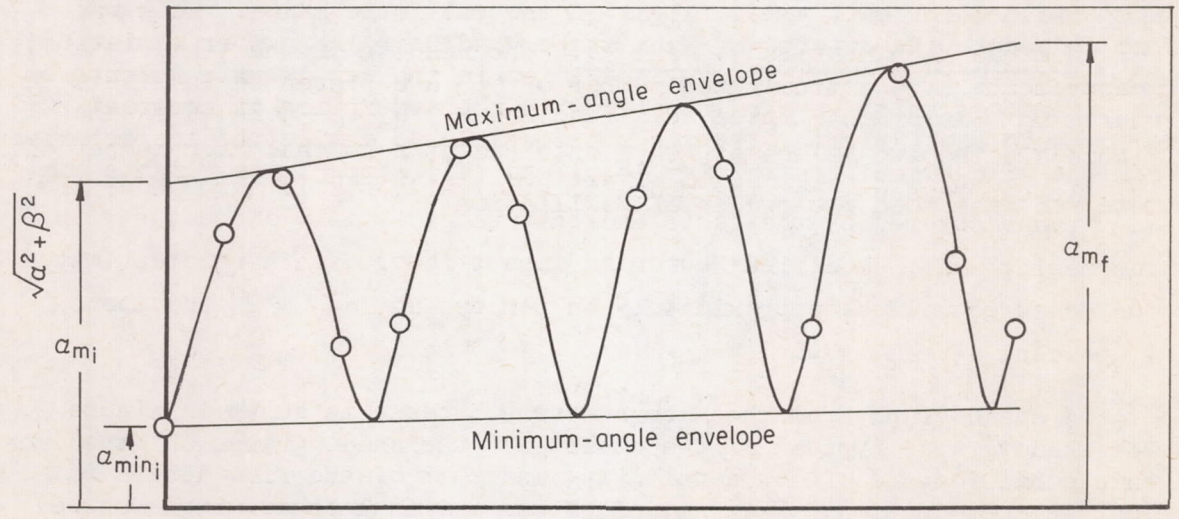

Sketch (a)

Static Stability

Nominal Mach number 3.- The results of the static-stability measurements at a nominal Mach number of 3 are presented in figure 5, where the pitching-moment-curve slope, C_{m_α}, is plotted as a function of the initial value of the maximum-angle envelope, α_{m_i}. The model was found to be statically stable for both center-of-gravity positions. It can be seen that the model is more stable at the higher Mach number and Reynolds number condition. The filled symbols in figure 5(a) are results from tests of a rough-faced model and will be discussed later. Included in figure 5 are values of C_{m_α} computed from modified Newtonian impact theory[2] which underestimates the measured values by about 50 percent.

The measured variation of stability with α_{m_i} seems to be associated with the flow conditions over the afterbody. The shadowgraphs show that at low angles of attack the flow was separated over the entire afterbody (see fig. 6(a)), and that as the angle increased the flow impinged on the windward side of the afterbody (see figs. 6(b) and (c)). (The parenthetic angles recorded in fig. 6 are the angles in the orthogonal plane.) At low angles of attack the stability decreases until the angle of attack becomes large enough to cause flow impingement; thereafter, the stability is increased.

Nominal Mach numbers 9.5 and 14.- The results of the static-stability measurements at a nominal Mach number of 9.5 are presented in figure 7, where C_{m_α} is again plotted as a function of α_{m_i}. Included in the figure are the two values of C_{m_α} obtained at a nominal Mach number of 14. It can be seen that the model is statically stable throughout the α_{m_i} range covered by the tests and that the stability decreases with increasing α_{m_i}. Modified Newtonian impact theory again underestimates the measured values, approximately 45 percent at $\alpha_{m_i} = 2^\circ$ and about 25 percent at $\alpha_{m_i} = 16^\circ$.

A shadowgraph from the Mach number 9.5 tests is shown in figure 8. The shadowgraph, typical of the quality of the shadowgraphs obtained at this condition, is of low sensitivity and most of the flow detail is lost in reproduction. Examination of the original shadowgraphs showed that at low angles of attack, the flow separated at the corner but then impinged on the cylindrical section. In contrast, at a Mach number of 3, the flow was completely separated over the entire afterbody (see fig. 6(a)). At higher angles of attack and a Mach number of 9.5, the flow appeared to be completely attached to the windward side (no flow impingement); whereas at a Mach number of 3, the flow separated at the

[2]The stagnation-pressure coefficient behind a normal shock wave was used in place of the coefficient 2.

2Y

DECLASSIFIED

corner and then impinged on the windward side. The different variations of C_{m_α} with α_{m_i} at the two Mach numbers is attributed to the difference in flow configurations over the afterbody.

Comments on flow details at nominal Mach number 5.- Two tests were conducted at a nominal Mach number of 5 for another investigation at the Ames Research Center. Though it was not possible to obtain stability data from the tests, it was felt that the flow details should be discussed. Two different Reynolds numbers were used: 1.8×10^6, which is comparable to the full-scale vehicle flight value, and 3.3×10^6. At the lower Reynolds number, the flow separated at the corner and impinged on the cylindrical section of the afterbody at low angles of attack. It will be recalled that at $M = 3$, $R = 2.2 \times 10^6$, the flow was completely separated over the afterbody at low angles of attack. Therefore, at a Reynolds number of about 2×10^6, the flow pattern changed from completely separated to impingement on the afterbody at some Mach number between 3 and 5. Further increase in Mach number from 5 to 14 had no significant effect on the flow pattern. For the other Mach number 5 test at the higher Reynolds number, 3.3×10^6, the flow was fully attached to the afterbody at low angles of attack. This is illustrated in figure 9, which is a shadowgraph from this test. It was suspected that the attached flow was caused by the increase in Reynolds number. However, calculations showed that the local Reynolds number at the maximum-diameter corner was about the same for this test and for the Mach number 3 tests where the flow was completely separated. There is a strong possibility, although it could not be definitely ascertained from the shadowgraphs, that the boundary layer was turbulent on the front face of the model with attached flow. This is in contrast to laminar flow off the front face of the models with separated flow. Flow attachment on or separation over the afterbody may be a function of the state of the boundary layer as it leaves the front face.

A 3 7 1

Attached flow at $M = 3$.- In order to determine whether a turbulent boundary layer on the model front face would induce flow attachment on the afterbody, a model with the front face roughened to promote turbulent flow was tested at a Mach number of 3. An undamaged model (fig. 10) recovered from the Mach number 3 tests had on its front face an imprint from a wire mesh screen which covered the model catcher. Since this roughness was considered more than sufficient to trip the boundary layer on the front face, the recovered model was tested at a nominal Mach number of 3 and Reynolds number of 2×10^6. Shadowgraphs from this test (flight no. 123) showed that the flow was turbulent and completely attached to the afterbody at low angles of attack. A comparison of the flow conditions over two models at the same Mach number, Reynolds number, and angle of attack (one model with a smooth front face, the other with a rough front face) is shown in the shadowgraphs of figure 11. The difference in the flow conditions over the afterbody is apparent. Turbulent flow over the front face did result in flow attachment to the afterbody

03741284030

at these test conditions. The amount of roughness required to promote turbulence over the front face was not investigated.

The static-stability results from flight number 123 are shown as filled symbols in figure 5(a). It can be seen that attached flow on the afterbody did not significantly affect the static stability of this configuration.

Dynamic Stability

The results of the dynamic-stability tests are presented in figure 12, where the dynamic-stability parameter, ξ, is plotted as a function of the initial value of the maximum-angle envelope, α_{m_i}. The model was found to be dynamically unstable at all conditions tested.

A 3 7 1

Nominal Mach number 3 tests.- Figure 12(a) shows the results from the Mach number 3 tests of the models with the forward center-of-gravity position. Included in the figure are the results from models with smooth (open symbols) and rough (filled symbols) front faces. The values of ξ vary from about 2 to 5 with one obvious exception, about 14. This extremely high value of ξ was measured from the test of the model with a rough front face (test no. 123, table I(a)). As was mentioned previously, the flow over this model was turbulent and completely attached to the afterbody at low angles of attack. This is in contrast to completely separated flow over the afterbody of the model with a smooth front face. The pitching and yawing motion of the rough-faced model (fig. 13) was similar to most of the motions of the smooth-faced models; that is, the motion showed thin precessing ellipses as viewed in the α - β plane. The higher value of ξ, 14.4, was obtained from the first part of the flight where the maximum angle of oscillation increased from about 7° to 19° in two cycles of oscillation; whereas the maximum-angle growth during the last part of the flight (ξ = 2.7) was much slower, increasing from about 17° to 22° in two cycles of oscillation. During the first part of the flight the flow was attached to the afterbody at low angles of attack. During the last part of the flight the flow was separated from the afterbody at low angles of attack. The attached flow observed during the first part of the flight was, therefore, an unstable flow pattern. The correspondence between unstable attached flow and high dynamic instability has been observed on other configurations (ref. 8). It is pointed out in the reference that with unstable attached flow, the high dynamic instability is a consequence of a hysteresis loop in the static pitching-moment curve. The possible presence of such a loop could not be determined from the present investigation since only the slope of the static pitching-moment curve was measured.

DECLASSIFIED

The data from the smooth-faced models (fig. 12(a)) show two values of ξ which are lower than the trend of the rest of the data from this model. Investigation revealed that the measured value of ξ was a function of the angle-of-attack range through which the model oscillated as well as the maximum angle of oscillation. The two points in figure 12(a) which fall below the faired curve were data from model motions which were more circular than the other motions as viewed in the $\alpha - \beta$ plane. A possible explanation of the lower values of ξ for the more circular motions is as follows. Unpublished preliminary data from the Langley Unitary Plan Wind Tunnel on tests of the Mercury re-entry capsule (although at a somewhat lower Mach number, 2.2) show a region of high dynamic instability near zero angle of attack. The two points in figure 12(a) which fall below the faired curve were data from model motions that had minimum angles of about 4° as compared to 1° or less for the other motions (see figs. 4(b) and 4(a) and column α_{m_i} in table I(a)). If a similar highly unstable region exists at Mach number 3, the flights with 4° minimum angles would be expected to have lower values of ξ than the flights with the same maximum angles which oscillated through or near zero angle of attack.

A 3 7 1

Figure 12(b) shows the dynamic-stability results from the Mach number 3 tests of the models with the aft center-of-gravity position. Also shown in the figure is the faired curve from figure 12(a). The data from the first part of the range flights, at the higher Mach number and Reynolds number, show a strong increase of instability with amplitude; whereas the data from the last parts at the lower Mach number and Reynolds number show a small variation of ξ with amplitude. This effect of Mach number and Reynolds number on the dynamic stability of the models with the aft center-of-gravity position did not appear in the data for the models with the forward center-of-gravity position. The reason for this is unknown but is believed not to be experimental error.

Nominal Mach number 9.5.- The dynamic-stability results of the Mach number 9.5 tests are presented in figure 12(c). As can be seen in the figure, the dynamic instability becomes less severe with increasing α_{m_i} at this Mach number. A comparison of these data with the Mach number 3 data (fig. 12(a)) shows that there is a strong dependence of ξ on Mach number as well as on α_{m_i}.

The value of ξ at $\alpha_{m_i} = 2^\circ$ is of lower reliability than the other data in figure 12(c). This is due to the fact that experimental errors in measuring angles of attack have larger effects on ξ in the low-angle range. For example, the estimated scatter in the angle measurements could alter the values of ξ in the higher α_{m_i} range by

03741284030

±5 percent; whereas the same amount of scatter could alter the value of ξ at $\alpha_{m_i} = 2^\circ$ by as much as ±25 percent. The trend of the data, however, (the increased instability at low angles) strengthens the conjecture mentioned previously in connection with the Mach number 3 data of a possible highly unstable region at low angles of attack.

A study of the shadowgraphs from the Mach number 9.5 tests showed that at low angles of attack the flow separated from the body at the maximum-diameter corner and then impinged and reattached on the cylindrical section of the body. It was deemed desirable to determine how the dynamic-stability characteristics would be affected if the corner were rounded to promote attached flow over the afterbody. One model with a rounded corner (corner radius equal to one-tenth of the maximum diameter) was tested at a Mach number of 9.96. It was extremely difficult to ascertain whether the flow was different from the flow over the basic configuration. The results from this one flight at $\alpha_{m_i} = 4.23^\circ$ showed considerably greater instability than the basic configurations, $\xi = 7.78$.

A 3 7 1

Drag

Drag coefficients were determined from the deceleration of the models by the procedure described in reference 9. These total-drag coefficients are plotted as a function of α_{m_i} in figure 14 and are tabulated in table I. Figure 14(a) shows the data from the Mach number 3 tests for both center-of-gravity positions. It can be seen that the drag decreases slightly with increasing α_{m_i}. Included in the figure are values of C_D computed from modified Newtonian impact theory. The theory is in good agreement with the measured values, about 5 percent high at $\alpha_{m_i} = 12^\circ$. Figure 14(b) shows the data from the Mach number 9.5 and 14 tests. Included in the figure are values of C_D computed from modified Newtonian impact theory. The theory overestimates the measured values by about 5 percent at $\alpha_{m_i} = 2^\circ$ and about 15 percent at $\alpha_{m_i} = 16^\circ$. When these data at Mach numbers 9.5 and 14 are compared with the data at Mach number 3 (fig. 14(a)) it can be seen that the drag is invariant with Mach number.

CONCLUDING REMARKS

Experimental measurements of the stability characteristics of the Mercury re-entry capsule in free flight at constant altitude have been made at Mach numbers from 3 to 14. Results of this investigation can be summarized as follows.

DECLASSIFIED

This configuration is dynamically unstable at Mach numbers near 3 and 9.5. The values of the dynamic-stability parameter range from about 1 to 6 for the design configuration when the flow was separated over the afterbody. At a Mach number of 3, a value of the dynamic-stability parameter of 14.4 was measured for a model with a roughened front face. The turbulent flow caused by the roughness resulted in a completely attached turbulent boundary layer on the afterbody. Not only was the dynamic stability adversely affected by the attached flow, but it can be presumed that the aerodynamic heating on both the front face and the afterbody would also be adversely affected. At a Mach number of 9.5, rounding the corner of a model to promote attached flow over the afterbody also adversely affected the dynamic stability.

A 3 7 1

The model is statically stable at Mach numbers from 3 to 14. The static stability was found to be a function of the flow conditions over the afterbody as well as the maximum angle of oscillation.

Ames Research Center
National Aeronautics and Space Administration
Moffett Field, Calif., April 19, 1960

REFERENCES

1. Sommer, Simon C., and Tobak, Murray: Study of the Oscillatory Motion of Manned Vehicles Entering the Earth's Atmosphere. NASA MEMO 3-2-59A, 1959.

2. Seiff, Alvin: A Free-Flight Wind Tunnel for Aerodynamic Testing at Hypersonic Speeds. NACA Rep. 1222, 1955.

3. Seiff, Alvin, and Sommer, Simon C.: An Investigation of Some Effects of Mach Number and Air Temperature on the Hypersonic Flow Over a Blunt Body. NASA MEMO 10-9-58A, 1959.

4. Nicolaides, John D.: On the Free Flight Motion of Missiles Having Slight Configurational Asymmetries. B.R.L. Rep. 858, Aberdeen Proving Ground, 1953.

5. Allen, H. Julian: Motion of a Ballistic Missile Angularly Misaligned With the Flight Path Upon Entering the Atmosphere, and Its Effect Upon Aerodynamic Heating, Aerodynamic Loads, and Miss Distance. NACA TN 4048, 1957.

6. Seiff, Alvin, Sommer, Simon C., and Canning, Thomas N.: Some Experiments at High Supersonic Speeds on the Aerodynamic and Boundary-Layer Transition Characteristics of High-Drag Bodies of Revolution. NACA RM A56I05, 1957.

7. Short, Barbara J., and Sommer, Simon C.: Some Measurements of the Dynamic and Static Stability of Two Blunt-Nosed, Low-Fineness-Ratio Bodies of Revolution in Free Flight at M = 4. NASA TM X-20, 1959.

8. Reese, David E., Jr., and Wehrend, William R., Jr.: An Investigation of the Static and Dynamic Aerodynamic Characteristics of a Series of Blunt-Nosed Cylinder-Flare Models at Mach Numbers from 0.65 to 2.20. NASA TM X-110, 1960.

9. Seiff, Alvin: A New Method for Computing Drag Coefficients From Ballistic Range Data. Jour. Aero. Sci., vol. 25, no. 2, Feb. 1958, pp. 133-134.

A 3 7 1

DECLASSIFIED

TABLE I.- TEST CONDITIONS AND FINAL DATA

Test number	M	$R \times 10^{-6}$	ξ	C_{m_α}	C_D	α_{m_1}, deg	α_{m_2}, deg	α_{min_1}, deg	$\frac{\omega d}{V}$	$\frac{x_{cg}}{d}$	d, in.	$\left(\frac{d}{\sigma}\right)^2$	$I_y \times 10^5$, slug-ft^2
(a) Nominal Mach number of 3, forward center-of-gravity position													
52-1	3.23	2.45	2.60	-0.247	1.53	4.90	5.89	1.01	0.018	0.347	1.650	6.88	2.59
52-2	2.61	1.98	2.85	-.222	1.53	5.99	7.48	1.37	.018	.347	1.650	6.88	2.59
53-1	3.21	2.44	4.13	-.263	1.52	8.75	11.82	1.13	.019	.348	1.650	6.88	2.59
53-2	2.58	1.96	4.75	-.267	1.52	11.71	17.07	.70	.019	.348	1.650	6.88	2.59
54-1	3.20	2.42	2.68	-.258	1.54	4.44	5.48	.45	.019	.348	1.650	6.96	2.58
54-2	2.62	1.98	3.25	-.232	1.54	5.38	6.79	.38	.018	.348	1.650	6.96	2.58
61-1	3.17	2.39	2.13	-.248	1.51	10.46	12.45	3.53	.019	.348	1.650	6.98	2.58
61-2	2.57	1.94	3.89	-.259	1.51	12.19	16.02	4.40	.019	.348	1.650	6.98	2.58
123-1	3.14	2.34	14.38	-.229	1.48	7.21	19.57	2.15	.018	.348	1.650	6.98	2.58
123-2	2.53	1.88	2.71	-.256	1.48	17.70	21.74	1.60	.019	.348	1.650	6.98	2.58
(b) Nominal Mach number of 3, aft center-of-gravity position													
89-1	3.02	2.48	2.52	-.216	1.53	5.32	6.45	.03	.017	.508	1.650	6.43	2.88
89-2	2.35	1.90	5.15	-.192	1.53	6.33	9.37	.07	.016	.508	1.650	6.43	2.88
90-1	2.96	2.37	1.97	-.255	1.55	2.97	3.48	.30	.018	.508	1.651	6.42	2.89
90-2	2.35	1.89	5.06	-.201	1.55	3.53	5.60	.50	.016	.508	1.651	6.42	2.89
91-1	3.00	2.39	4.58	-.225	1.51	6.59	9.03	1.18	.017	.509	1.650	6.41	2.89
91-2	2.39	1.90	5.74	-.227	1.51	9.56	14.86	.97	.017	.509	1.650	6.41	2.89
98-1	3.03	2.39	5.00	-.239	1.52	7.78	11.14	1.96	.017	.513	1.651	6.34	2.94
98-2	2.48	1.97	5.05	-.239	1.52	10.74	15.82	2.52	.017	.513	1.651	6.34	2.94
(c) Nominal Mach number of 9.5, forward center-of-gravity position													
479	9.58	1.44	1.34	-.239	1.54	6.28	6.71	1.08	.013	.359	.450	6.94	3.93
480	9.32	1.40	1.20	-.217	1.52	9.61	10.18	.64	.012	.360	.450	6.95	3.88
501	9.80	1.44	0.86	-.179	1.44	21.11	21.72	.70	.011	.358	.450	6.91	3.92
506	9.22	1.35	4.86	-.264	1.56	1.88	2.38	1.23	.013	.358	.450	6.80	3.97
518	9.54	1.38	1.60	-.240	1.50	5.38	5.89	2.70	.012	.361	.450	6.87	3.94
(d) Nominal Mach number of 14, forward center-of-gravity position													
573	14.37	1.94	--	-.177	1.43	24.00	--	4.00	.010	.358	.451	6.87	3.96
576	13.89	1.94	--	-.190	1.52	12.30	--	.40	.011	.358	.450	6.89	3.96

0317126J030

A 3 7 1

3Y

DECLASSIFIED

A 3 7 1

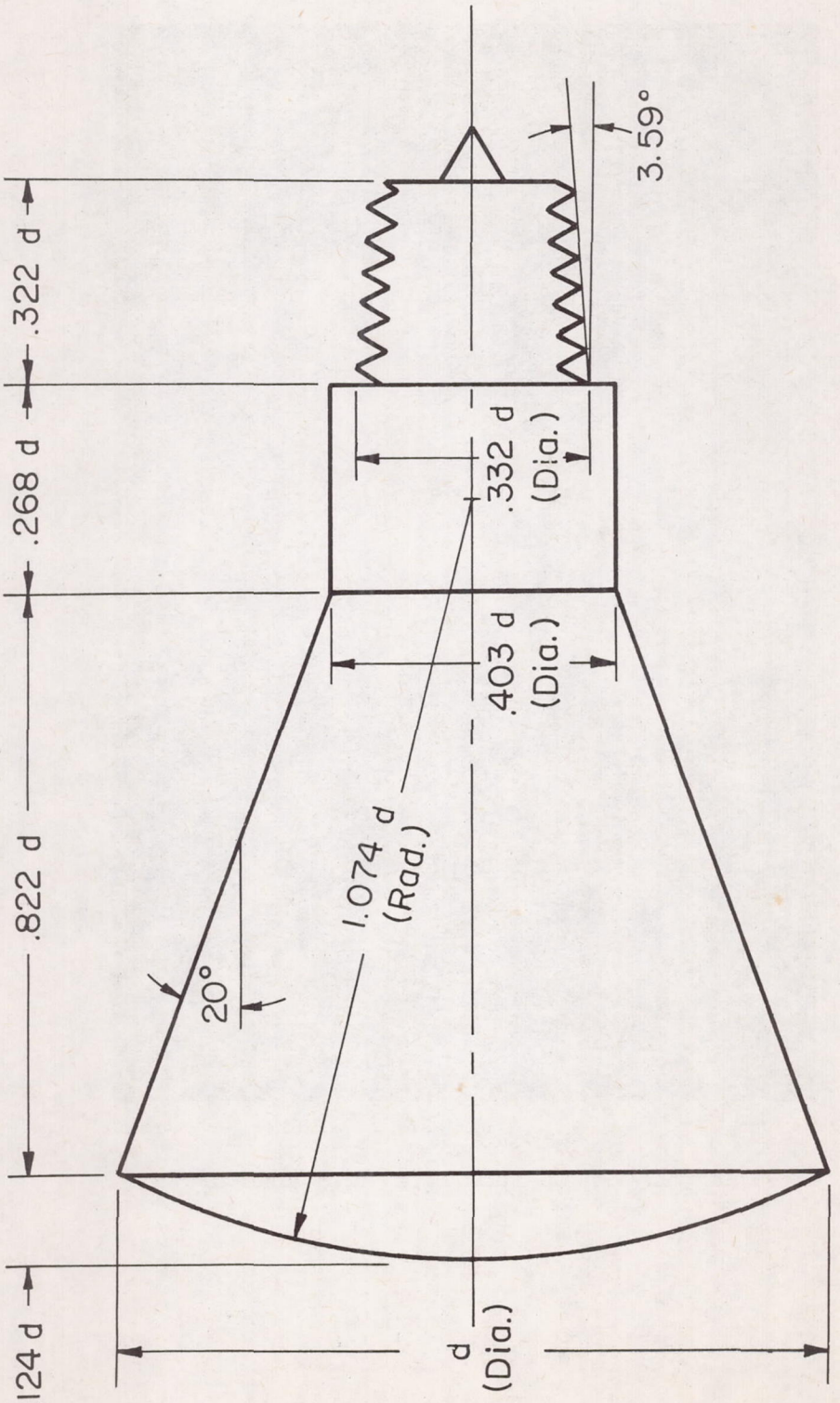

Figure 1.- Sketch of model.

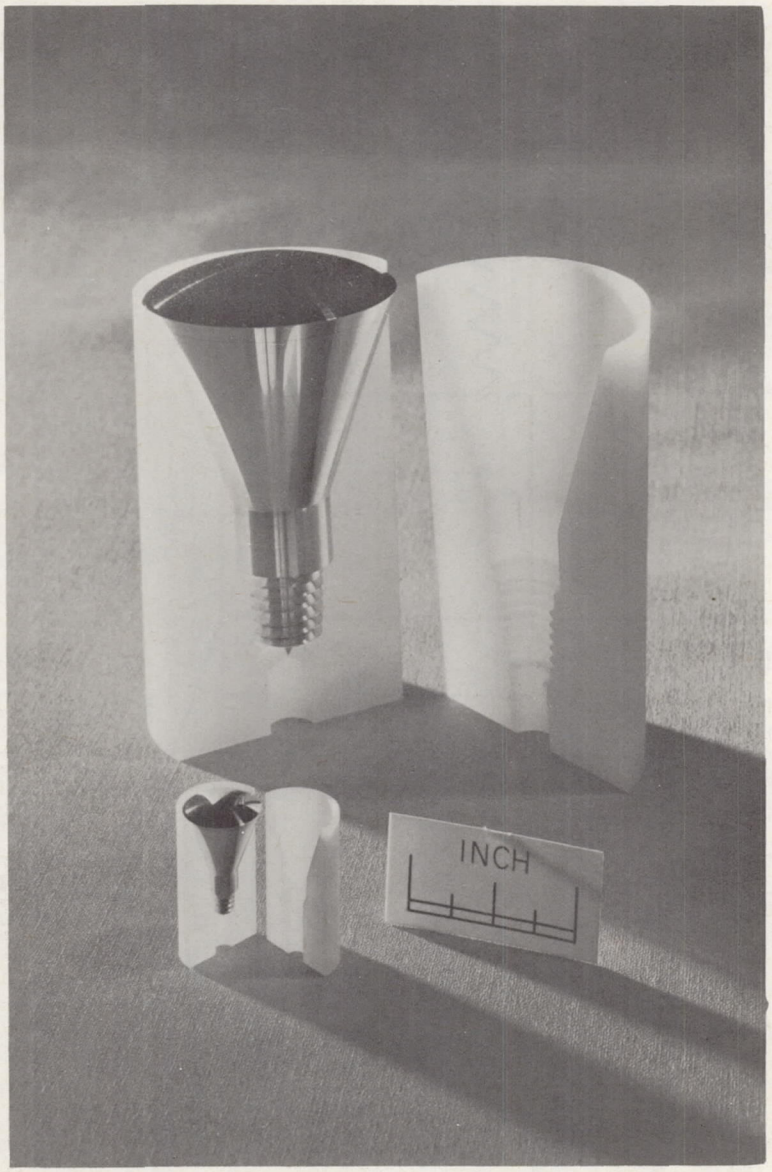

A-25041

Figure 2.- Photograph of models and sabots.

CONFIDENTIAL

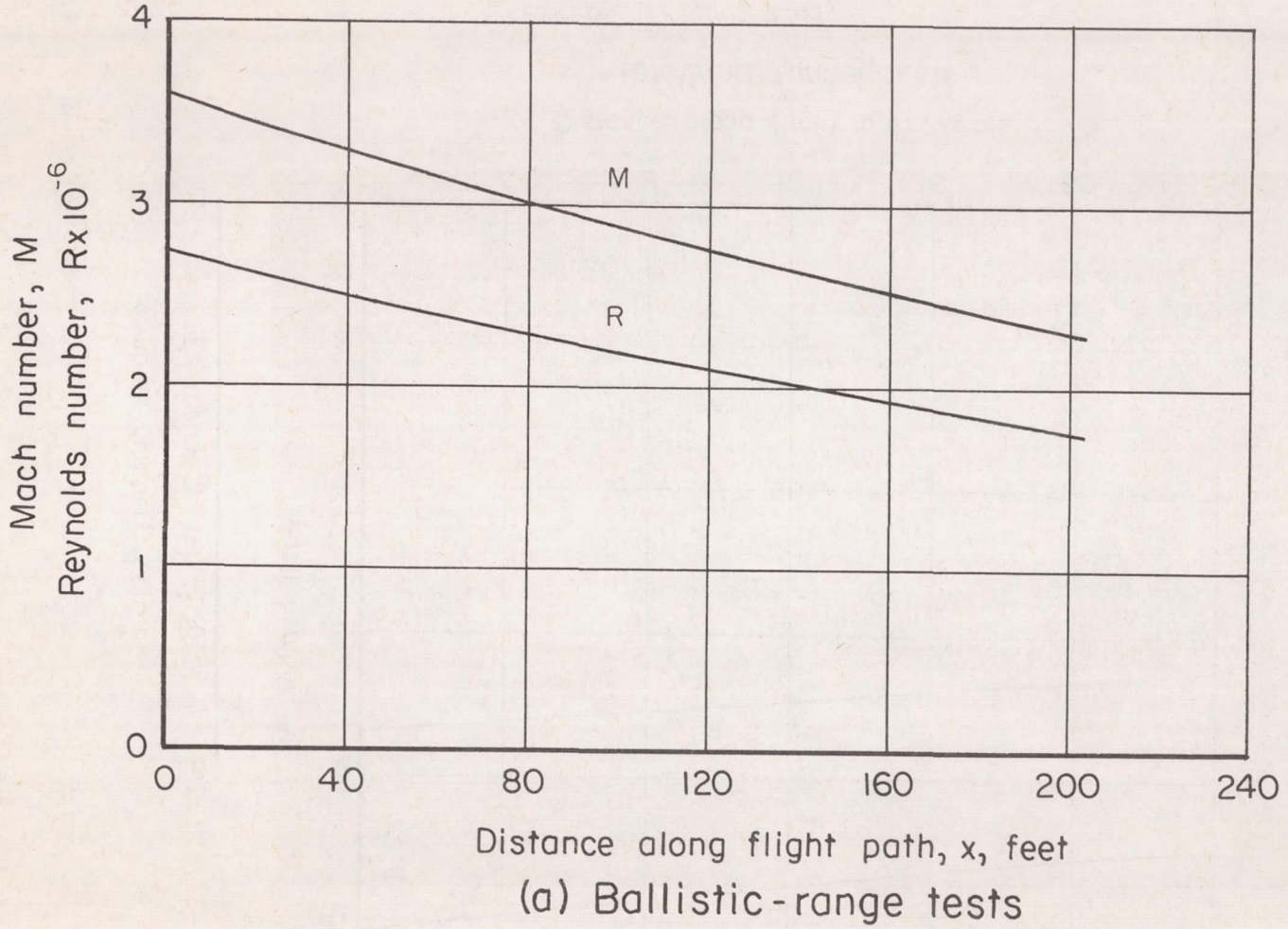

Figure 3.- Typical Mach number and Reynolds number variations.

CONFIDENTIAL

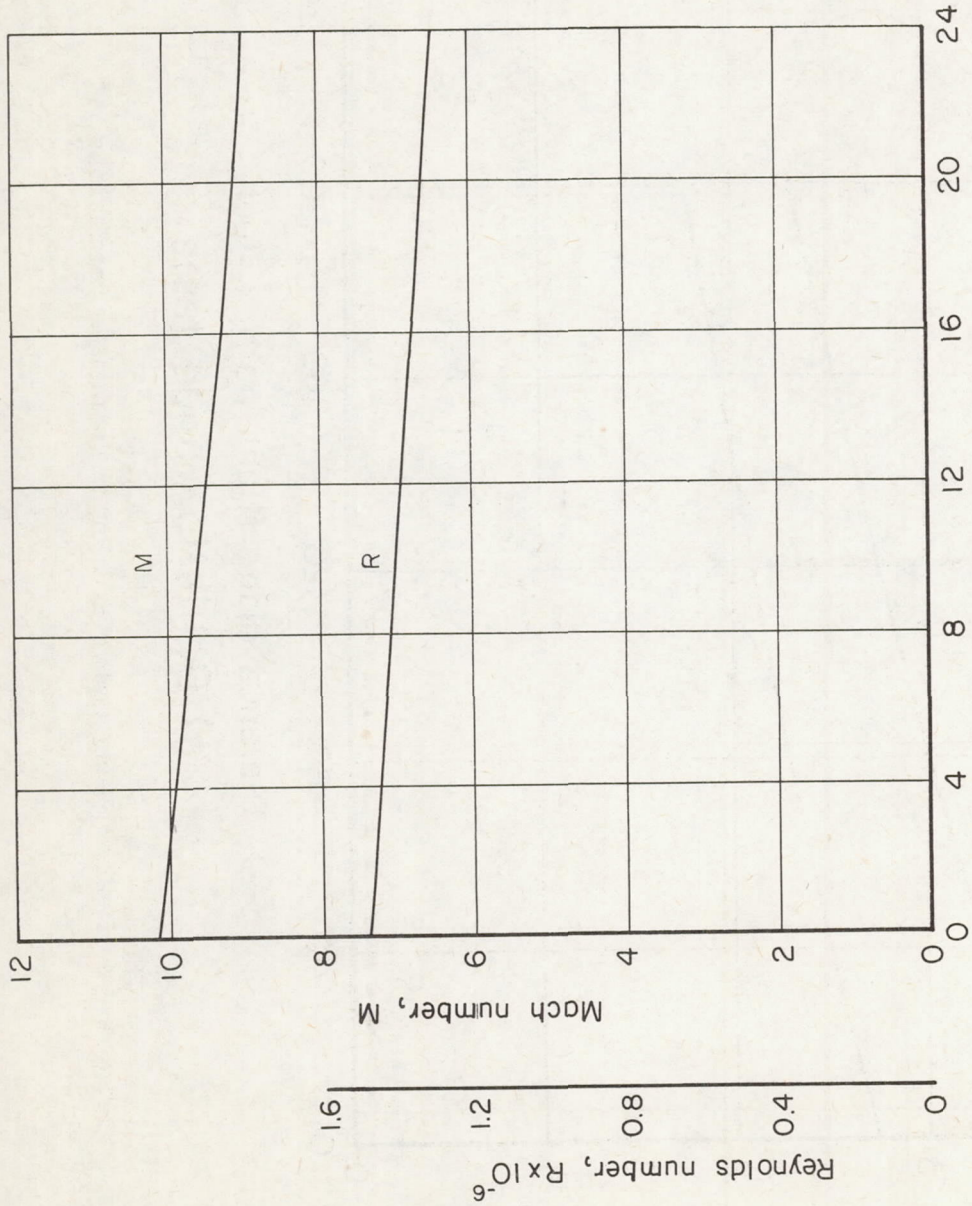

(b) Wind-tunnel tests

Figure 3.- Concluded.

CONFIDENTIAL

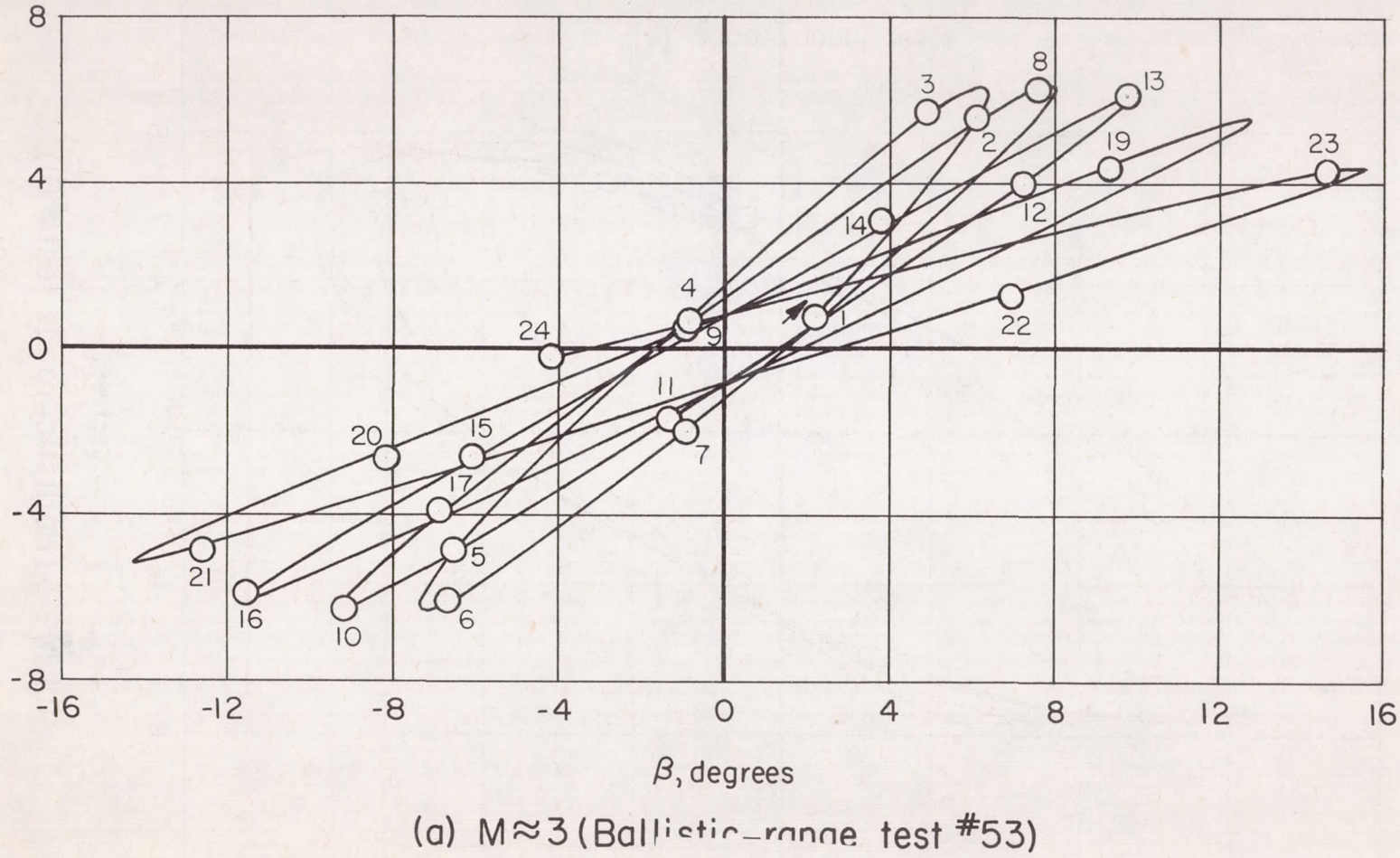

(a) M≈3 (Ballistic-range test #53)

Figure 4.- Typical pitching and yawing motions.

CONFIDENTIAL

0317124J030

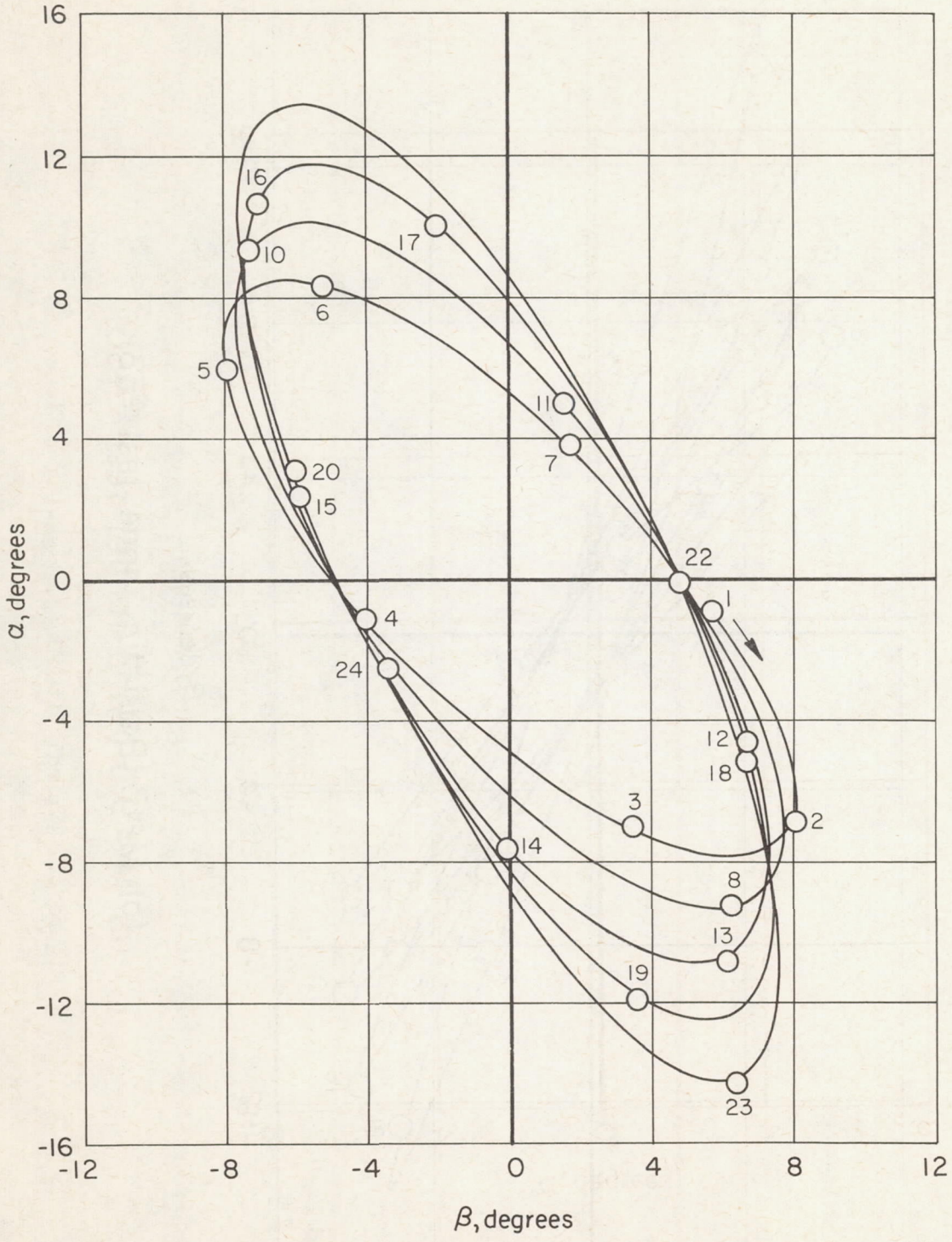

(b) M≈3 (Ballistic-range test #61)

Figure 4.- Continued.

A 3 7 1

DECLASSIFIED

A
3
7
1

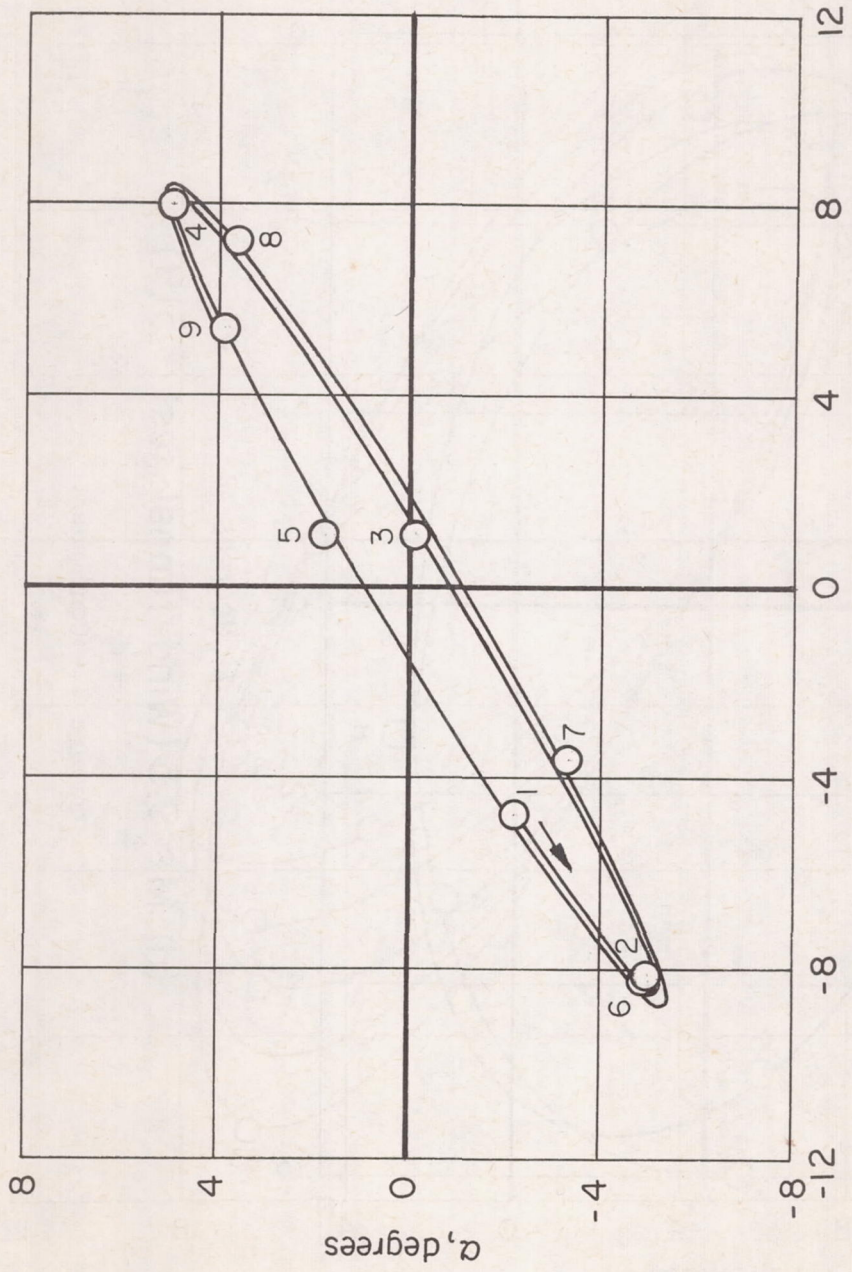

(c) M≈9.5 (Wind-tunnel test #480)

Figure 4.- Continued.

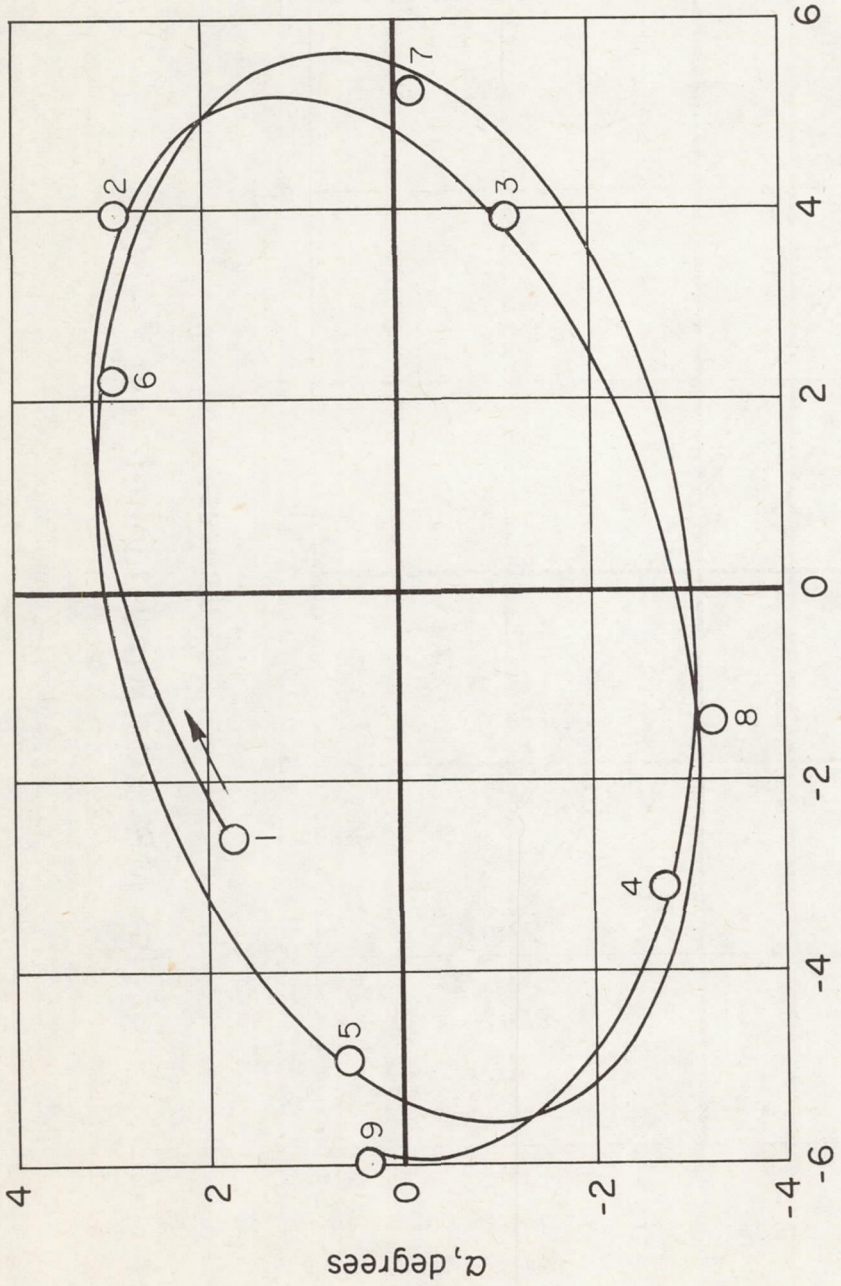

(d) M≈9.5 (Wind-tunnel test #518)

Figure 4.- Concluded.

A 3 7 1

4Y

DECLASSIFIED

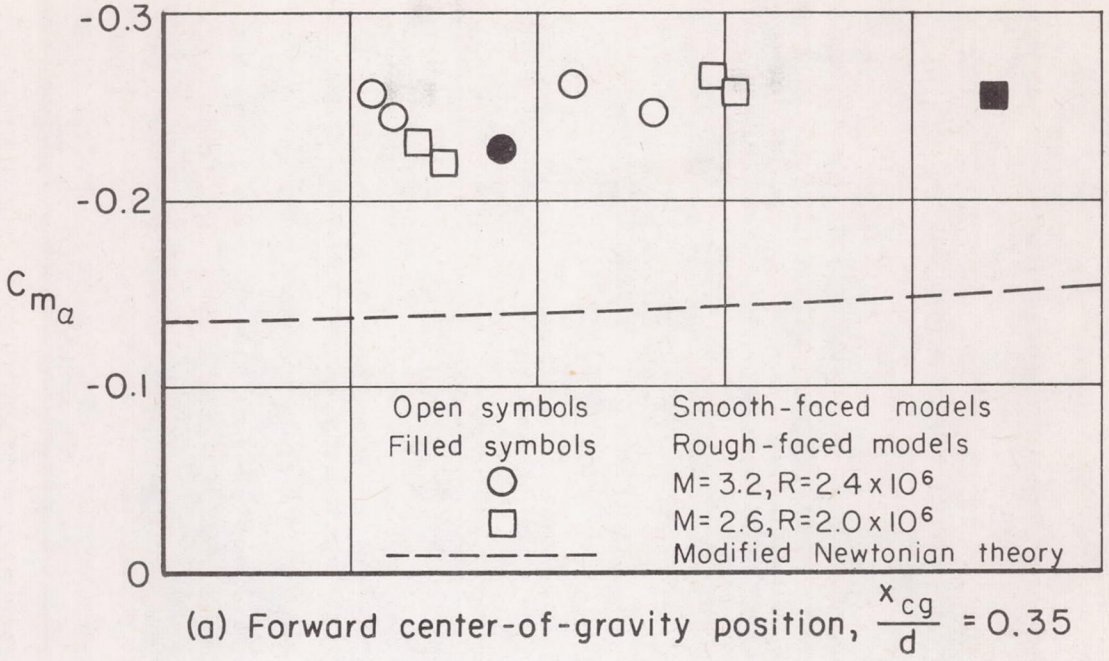

(a) Forward center-of-gravity position, $\frac{x_{cg}}{d} = 0.35$

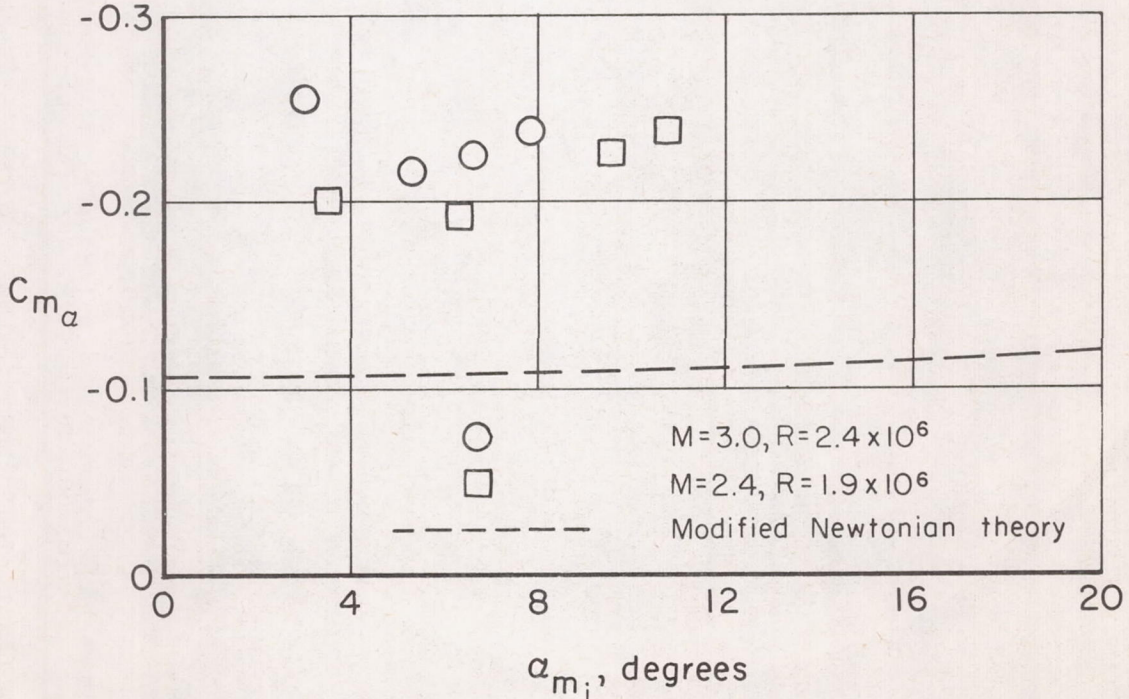

(b) Aft center-of-gravity position, $\frac{x_{cg}}{d} = 0.51$

Figure 5.- Static-stability results at a nominal Mach number of 3.

CONFIDENTIAL

A-25027

(a) Separated flow, $\alpha = 0.7^{\circ}$ ($\beta = 0.9^{\circ}$), M = 3.44, R = 2.62×10^{6}.

Figure 6.- Typical shadowgraphs from ballistic-range tests at a nominal Mach number of 3.

CONFIDENTIAL

NACA RM A53L17

A-25028

(b) Flow impingement, $\alpha = 6.3^{\circ}$ ($\beta = 9.2^{\circ}$), M = 3.03, R = 2.31×10^{6}.

Figure 6.- Continued.

CONFIDENTIAL

CONFIDENTIAL

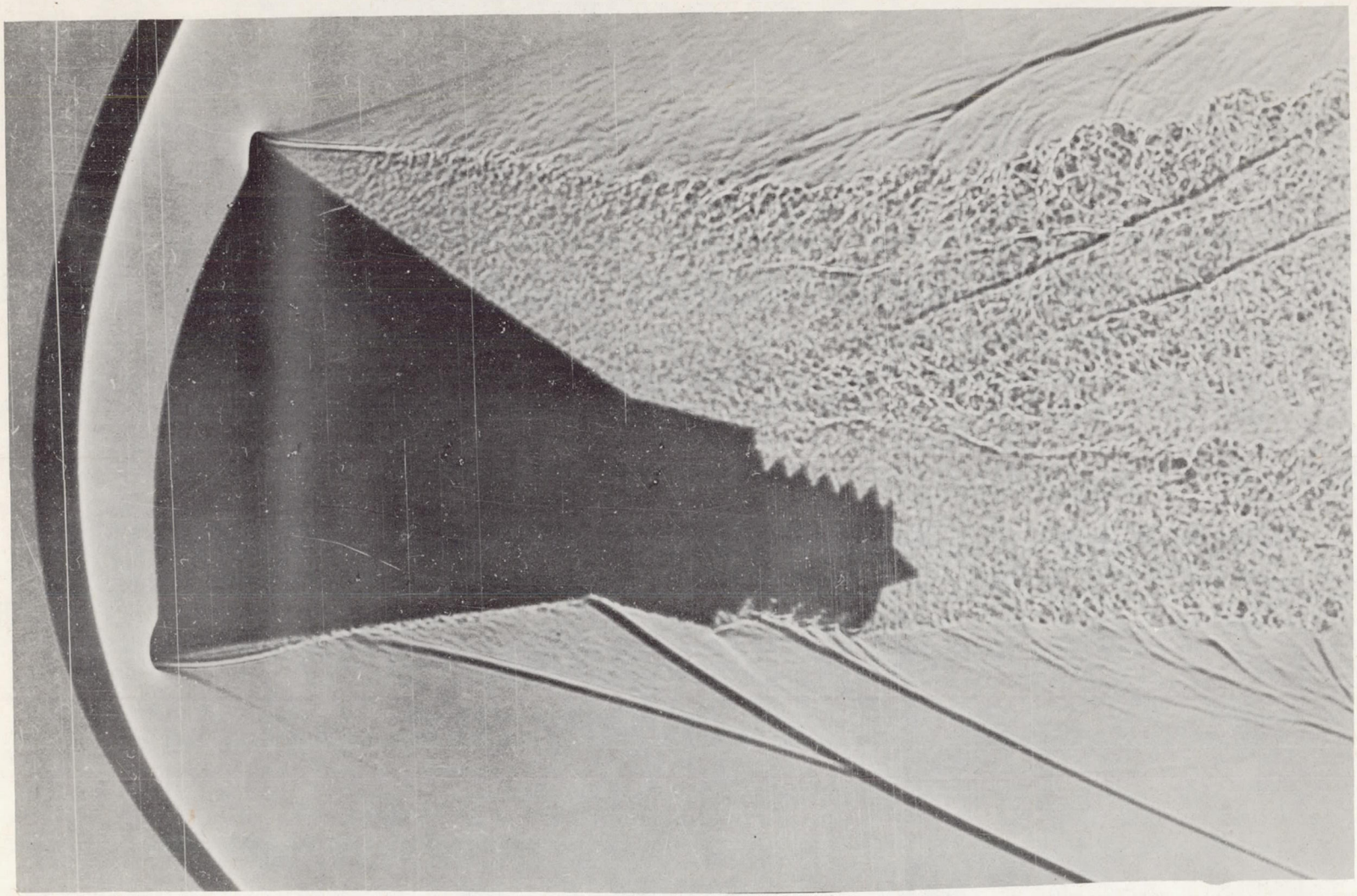

A-25029

(c) Flow impingement, $\alpha = 14.6^{\circ}$ ($\beta = 4.3^{\circ}$), M = 2.34, R = 1.78×10^{6}.

Figure 6.- Concluded.

CONFIDENTIAL

A 3 7 1

A 3171

CONFIDENTIAL

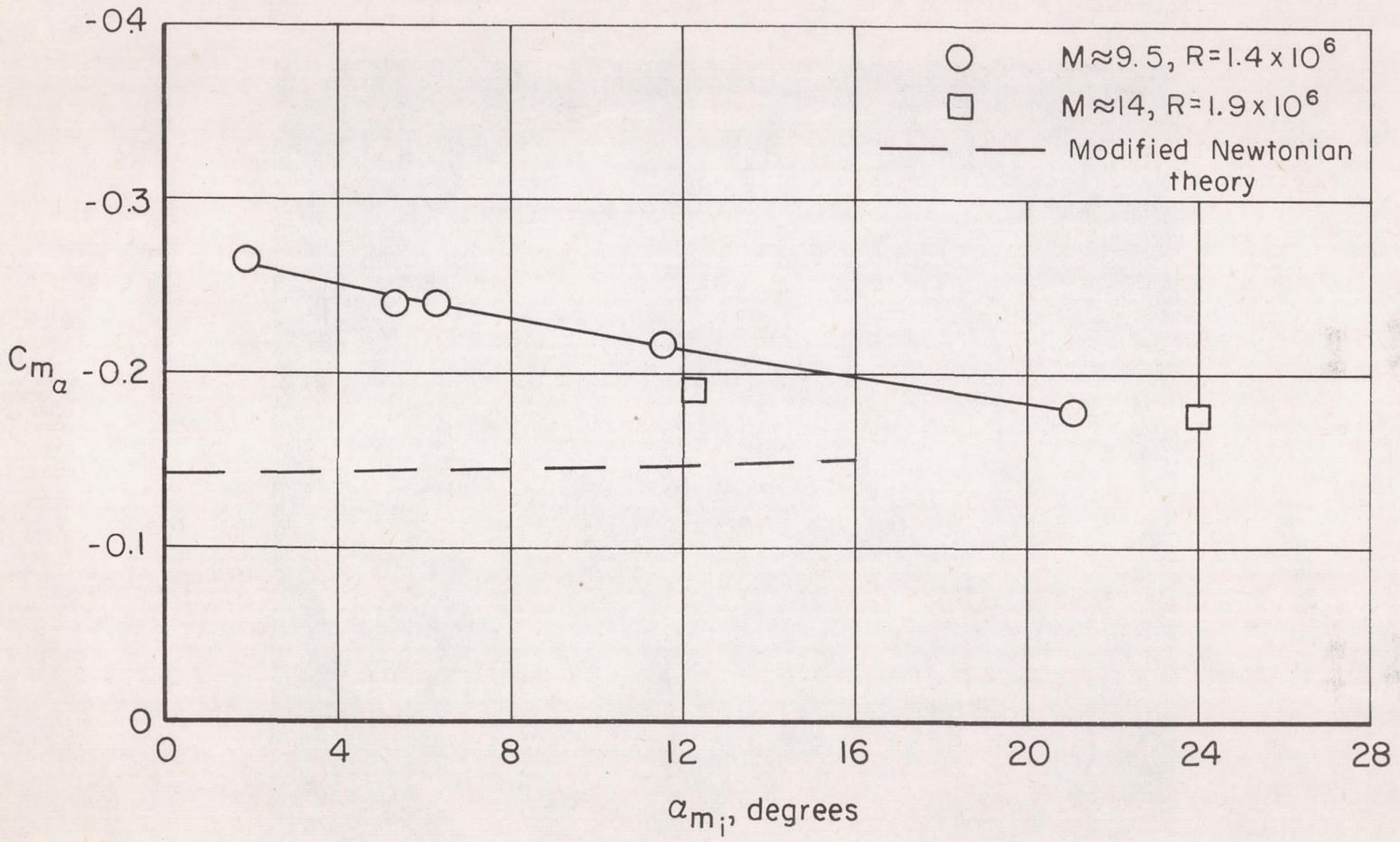

Figure 7.- Static-stability results at a nominal Mach number of 9.5; $x_{cg}/d = 0.36$.

CONFIDENTIAL

CONFIDENTIAL

A-25025

Figure 8.- Typical shadowgraph from wind-tunnel tests, $\alpha = 0.8^{\circ}$ ($\beta = 1.3^{\circ}$), $M = 9.75$, $R = 1.47 \times 10^{6}$.

CONFIDENTIAL

A 3 7 1

DECLASSIFIED

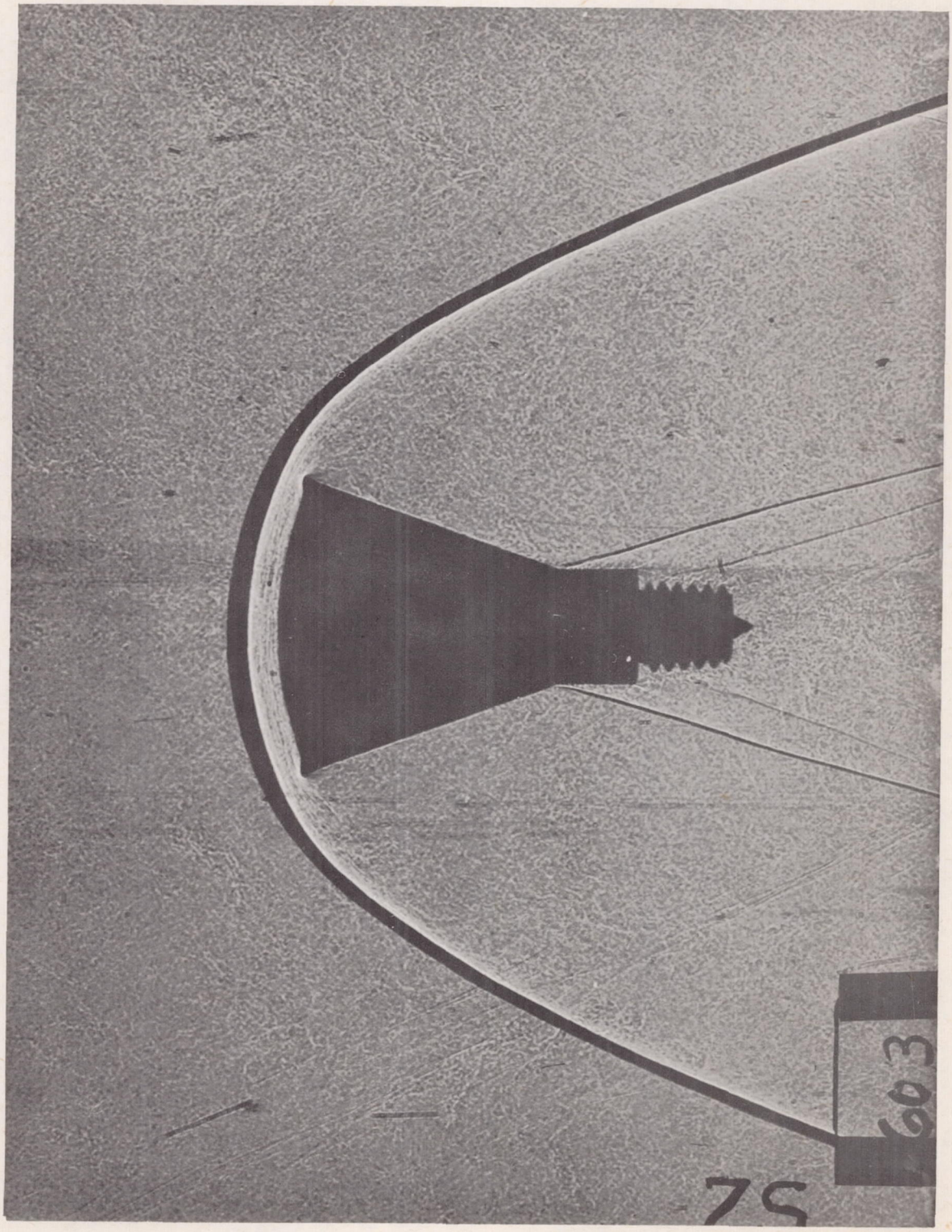

A-26040

Figure 9.- Shadowgraph of model with attached flow, $\alpha = 0.5^{\circ}$ ($\beta = 4.0^{\circ}$), $M = 5.34$, $R = 3.31 \times 10^{6}$.

CONFIDENTIAL

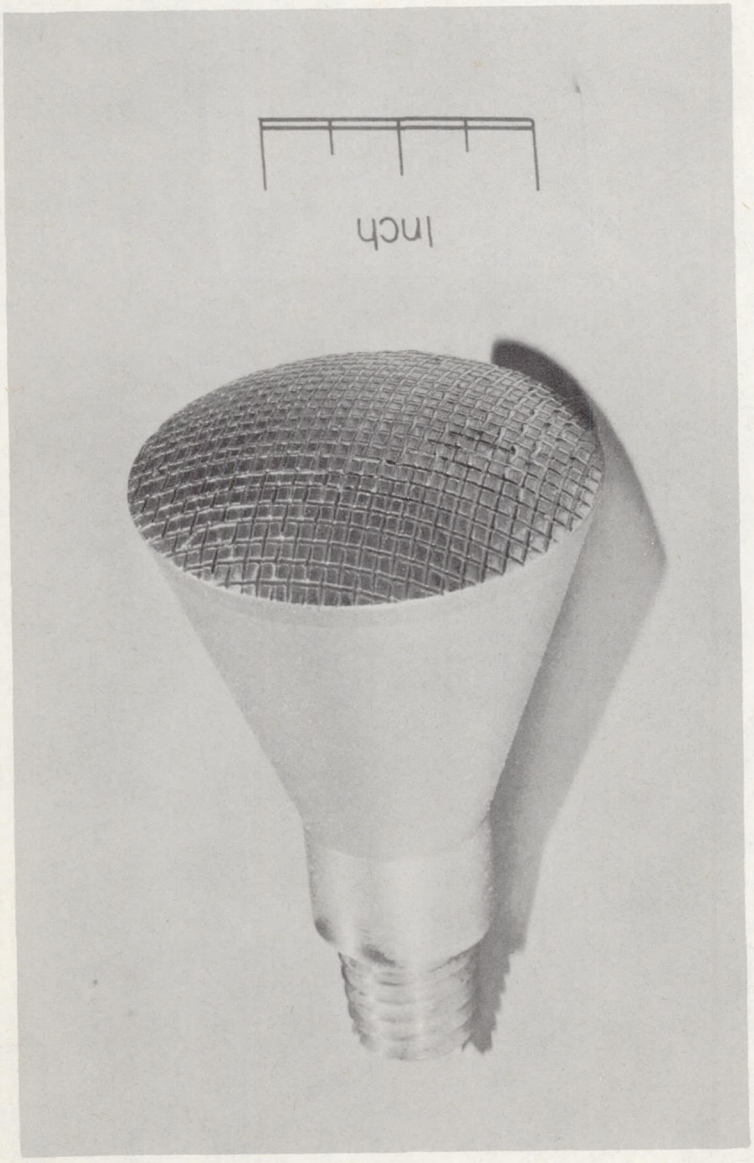

A-26346

Figure 10.- Photograph of model with rough front face

A 3 7 1

CONFIDENTIAL

5Y

DECLASSIFIED

A
3
7
1

CONFIDENTIAL

A-26341

(a) Separated flow (smooth-faced model), $\alpha = 2.0^{\circ}$ ($\beta = 0.9^{\circ}$), M = 3.28, R = 2.50×10^{6}.

Figure 11.- Comparison of flow details for smooth- and rough-faced models at the same test conditions.

CONFIDENTIAL

CONFIDENTIAL

CONFIDENTIAL

A-26343

(b) Attached flow (rough-faced model), $\alpha = 2.4^{\circ}$ ($\beta = 0.9^{\circ}$), M = 3.28, R = 2.44×10^{6}.

Figure 11.- Concluded.

CONFIDENTIAL

0 3 1 9 1 2 2 4 1 0 3 0

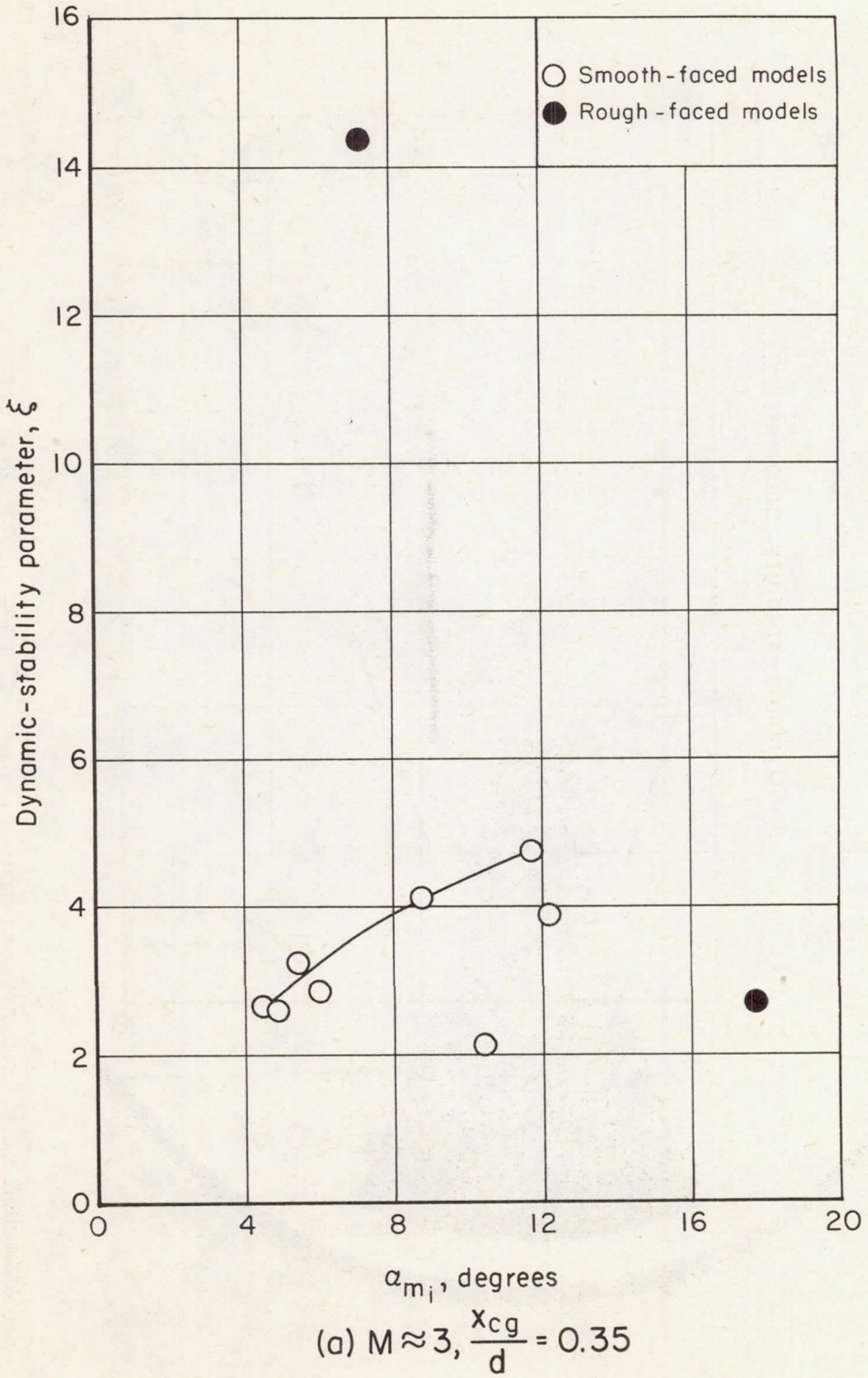

Figure 12.- Dynamic-stability results.

A 3 7 1

DECLASSIFIED

A
3
7
1

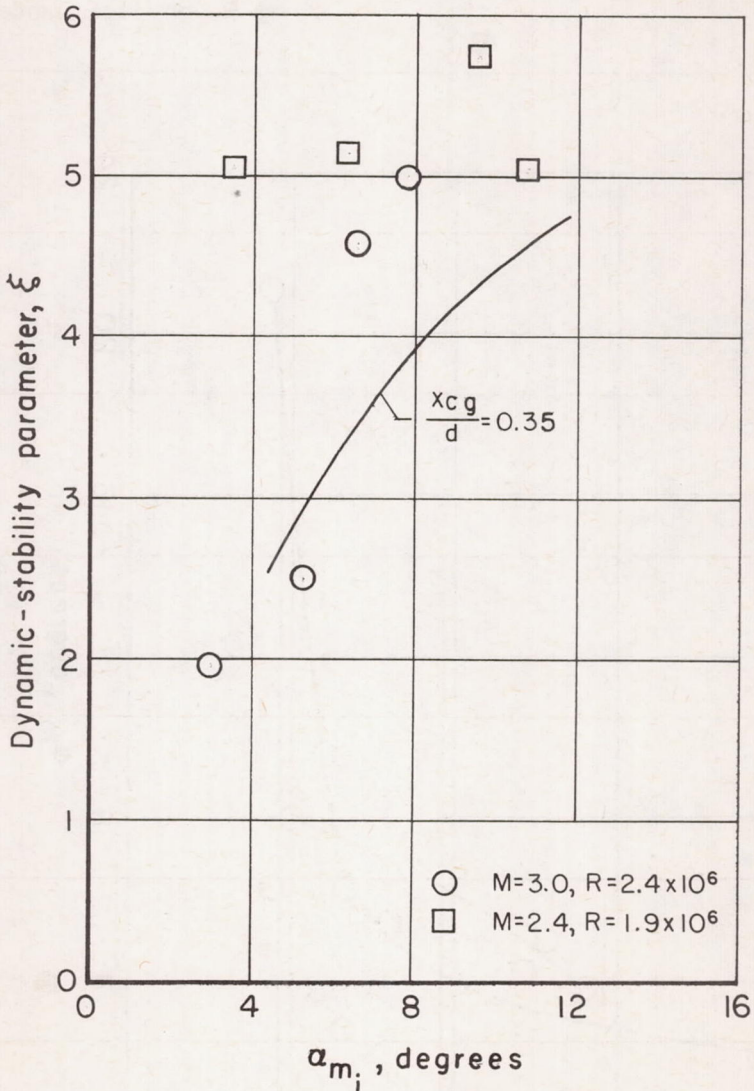

(b) $M \approx 3$, $\frac{x_{cg}}{d} = 0.51$

Figure 12.- Continued.

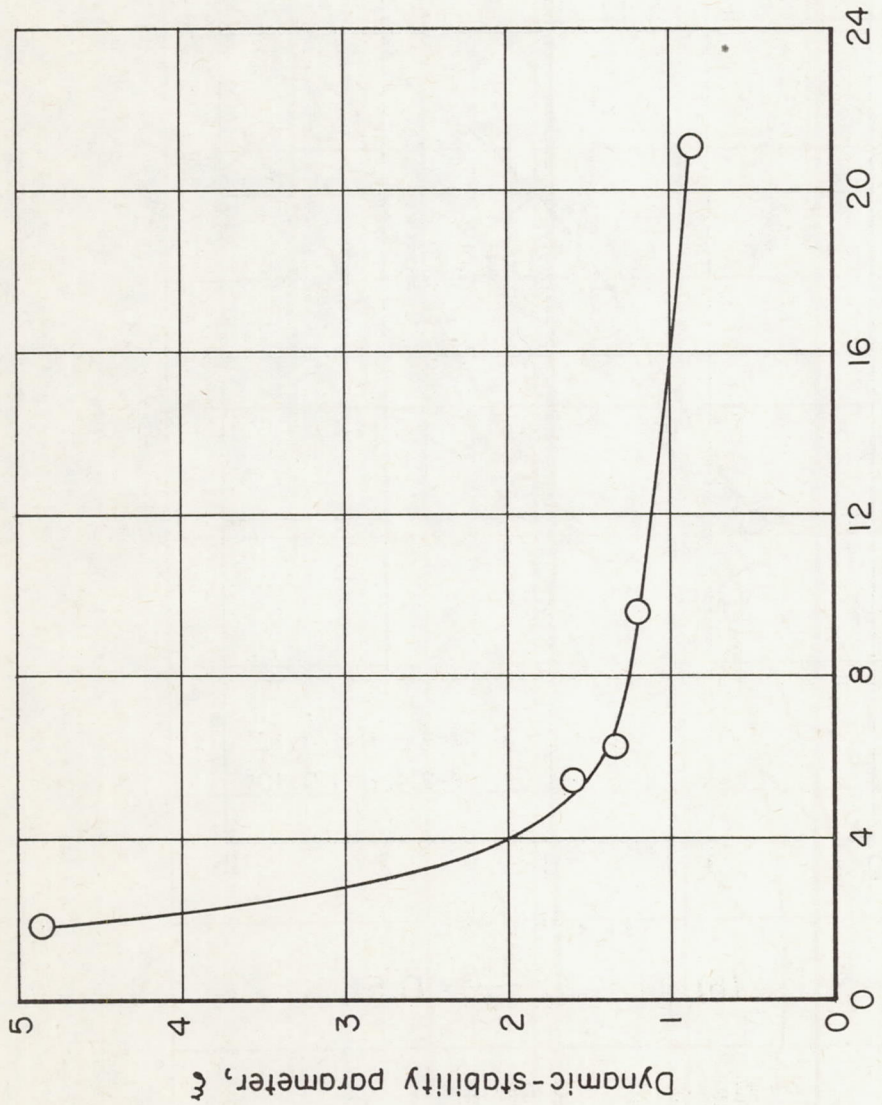

(c) $M \approx 9.5, \frac{x_{cg}}{d} = 0.36$

Figure 12.- Concluded.

DECLASSIFIED

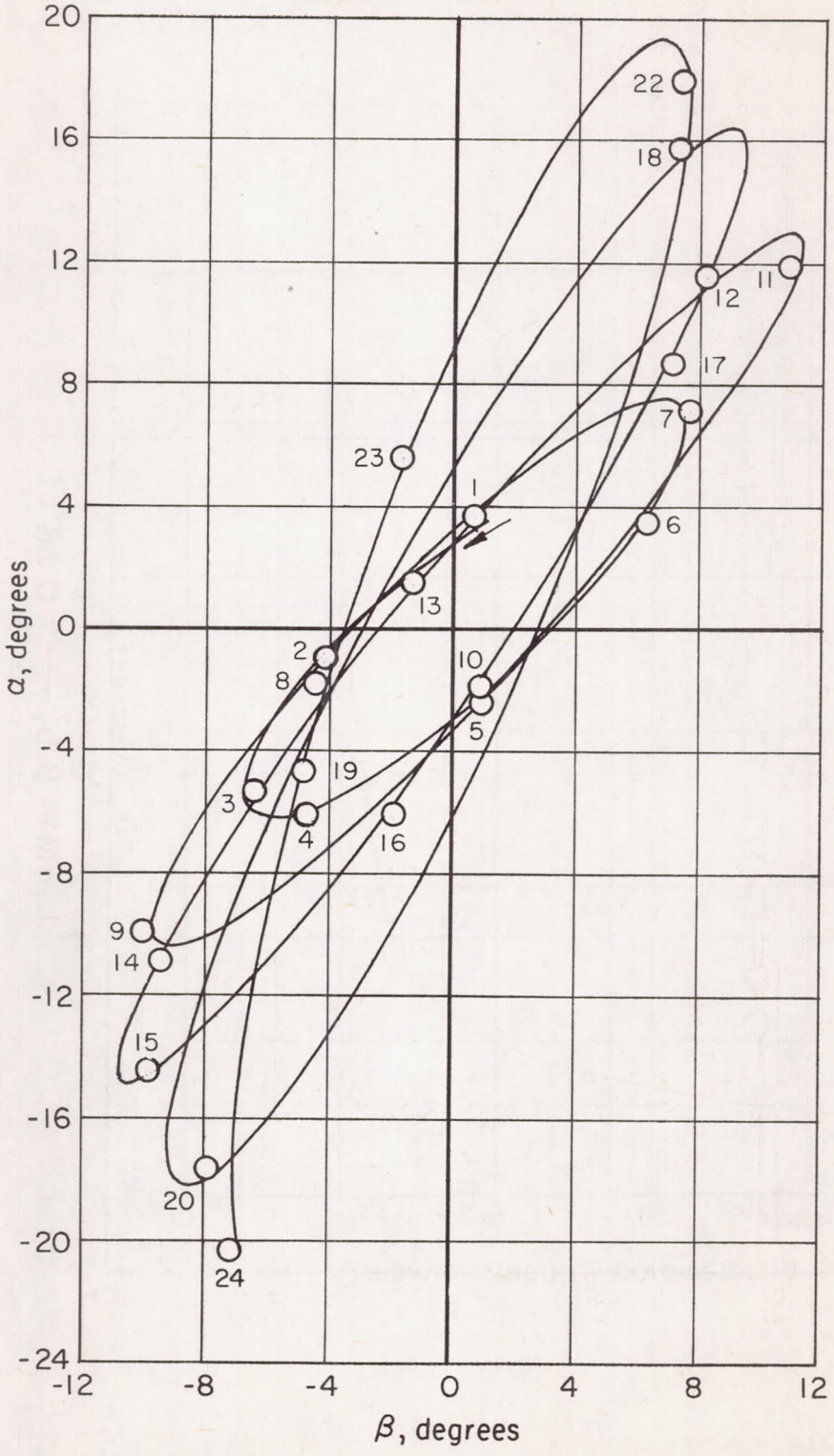

Figure 13.- Pitching and yawing motion of rough-faced model (test no. 123).

CONFIDENTIAL

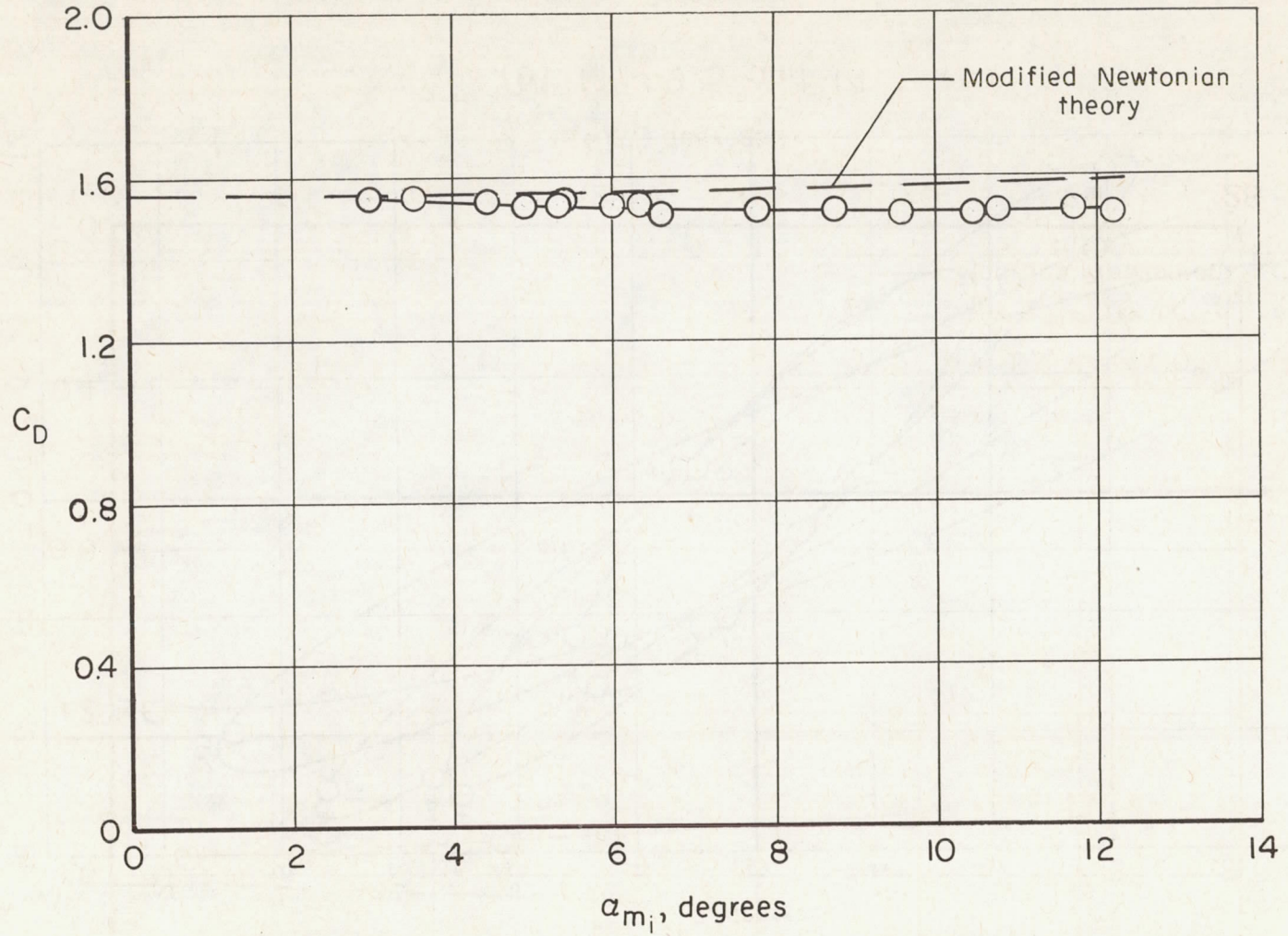

(a) $M \approx 3$

Figure 14.- Drag results.

CONFIDENTIAL

NASA - Langley Field, Va. A-371 CONFIDENTIAL

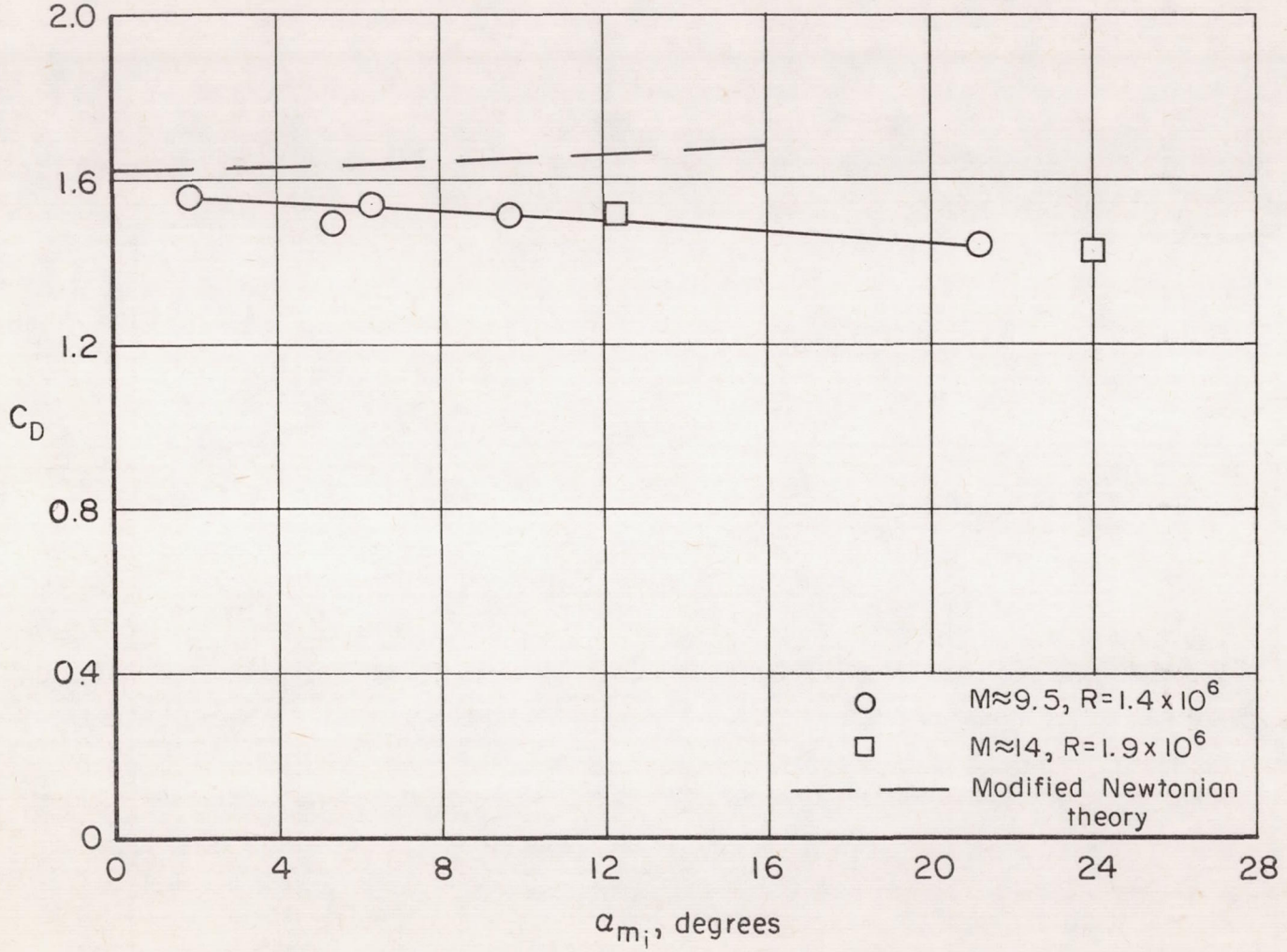

(b) M ≈ 9.5 and 14

Figure 14.- Concluded.

CONFIDENTIAL

D3179122A1030

DECLASSIFIED

CONFIDENTIAL

CONFIDENTIAL